A Case Study of Downstream Baroclinic Development over the North Pacific Ocean. Part II: Diagnoses of Eddy Energy and Wave Activity

Richard E. Danielson, John R. Gyakum, and David N. Straub

Atmospheric and Oceanic Sciences, McGill University, Montreal, Quebec, Canada

(Manuscript received 14 March 2005, in final form 31 August 2005)

ABSTRACT

The sequential development of a western, and then an eastern, North Pacific cyclone is examined in terms of eddy energy and a phase-independent wave activity. Based on the propagation of both a contiguous wave activity center and eddy energy, the development of the western cyclone appears to influence its downstream neighbor. A quantitative comparison of these two diagnoses is made in terms of group velocity, and only minor differences are found during much of the initial evolution. It is only once the tropopause undulations lose their wavelike appearance (at which point, application of the group-velocity concept itself becomes quite tenuous) that the downstream propagation of eddy energy seems faster than that of wave activity. Conventional methods of tracking this wave packet are also briefly discussed.

1. Introduction

There is growing evidence that the development of midlatitude cyclones and anticyclones can be attributed in part to the propagation of wave packets toward them (Joung and Hitchman 1982; Orlanski and Sheldon 1993; Chang 2000). A wave packet is broadly defined as a localized series of upper-level troughs and ridges whose amplitude is maximized near the center. Orlanski and Katzfey (1991) discovered that the ageostrophic geopotential flux, which defines an important part of the propagation of eddy energy, can be used to track a wave packet as it moves downstream. An account of the work leading to this interpretation is given by Chang (2000). Although the physical interpretation of other eddy energy budget terms may be well established, it is also well known that energy flux and conversion terms are not uniquely defined (Longuet-Higgins 1964; Plumb 1983). This complicates a ranking of the processes resolved by an eddy energy budget and, in particular, an estimate of the relative importance of wave packet propagation. An alternative approach is to consider a wave activity (e.g., Takaya and Nakamura 2001), whose budget terms can be uniquely defined. The evolution of a wave packet may also be simpler to diagnose using this quantity because it is conserved in the absence of diabatic and frictional processes, whereas eddy energy is not.

Midlatitude wave packets have been examined by Lee and Held (1993), Chang (1993), Chang and Yu (1999), and Hakim (2003). These studies revealed that the downstream movement of wave packets is invariably faster than the propagation of troughs and ridges. It follows that individual troughs and ridges defining a wave packet tend to be dynamically dependent on their upstream neighbors. This sequential growth and decay of adjacent troughs and ridges is known as downstream development. Some indication that downstream development is important for the development of particular cyclones is found in the local eddy energy diagnoses of Orlanski and Katzfey (1991) and Orlanski and Sheldon (1995). These studies employed the ageostrophic geopotential flux to resolve the radiation of eddy energy between adjacent troughs and ridges. A well-known ambiguity in the diagnosis of energy propagation, however, is that the flux is not unique. Only the divergence of this flux contributes to the local energy tendency (Longuet-Higgins 1964). Under certain assumptions, this ambiguity can be removed by stipulating that the flux, when normalized by eddy energy and integrated over wave phase, is equal to the group velocity (Pedlosky 1987). Although such assumptions may not always be justified, the direction given by such a flux is

Corresponding author address: Rick Danielson, Department of Oceanography, Dalhousie University, 1355 Oxford Street, Halifax NS B3H 4J1, Canada.
E-mail: rick@phys.ocean.dal.ca

generally a reasonable indication of the direction of wave packet propagation.

The quasigeostrophic version of the eddy ageostrophic geopotential flux was given by Chang and Orlanski (1994), who indicated that this flux is parallel to the group velocity relative to a uniform zonal flow. In this context, the eddy energy flux is uniquely defined and its physical interpretation is unambiguous, but when diagnosing observed events, it is also convenient to measure the importance of downstream development. Typically, such a measure is obtained by comparing the flux divergence term to other terms of the energy budget. Plumb (1983) emphasized, however, that none of the conversions and fluxes of an energy budget are necessarily unique. Without a physical justification for the form of the other energy budget terms, it is difficult to claim that the flux divergence term is most important. This is a diagnostic challenge that can be met by employing a quantity that is strictly conserved in the absence of diabatic and frictional forcing. When such a quantity of the flow can be defined (e.g., Edmon et al. 1980; Plumb 1986; Takaya and Nakamura 2001), its budget is written in the form

$$\frac{\partial A}{\partial t} + \nabla \cdot \mathbf{F} = S, \tag{1}$$

where A is called a wave activity, $\mathbf{F}$ is its flux, and S is associated with the nonconservative forcing of the waves. The Eliassen–Palm flux (Edmon et al. 1980) is an example of $\mathbf{F}$ that illustrates the propagation of disturbances on a zonal mean flow. As with eddy energy flux, not all definitions of wave activity flux satisfy the group-velocity property [although we focus on a wave activity that does in this study (cf. Vanneste and Shepherd 1998)]. Unlike eddy energy, however, when the interpretation of the flux is constrained by the group-velocity property, it is convenient that the other wave activity budget terms have rather direct physical interpretations.

If the eddy energy budget is expressed in the form (1), then S is associated with nonconservative eddy forcing and conversions between different forms of energy. In the midlatitudes, these conversions arise primarily because the basic state is zonally and vertically varying. Chang and Orlanski (1994) demonstrated that the ageostrophic geopotential flux is close to the group velocity in idealized linear shear flows by computing the flux and group velocity for models with vertically varying basic states. They claimed that the full geopotential flux is consistent with the observational analysis of Chang (1993), implying that it can be used to indicate eddy energy propagation for both vertically and zonally varying nonlinear flows. What Chang and Orlanski (1994) left open is the question of whether a locally defined group velocity can be defined for a zonally varying basic state. An expression for such a quantity was given by Takaya and Nakamura (2001, hereafter TN01) for small-amplitude quasigeostrophic eddies. They found that by combining a normalized eddy energy and eddy enstrophy, a spatial average as in Edmon et al. (1980), or a temporal average as in Plumb (1986), is unnecessary to derive a wave activity equation of the form (1). The result is that a wave activity and its flux (and hence, group velocity) can then be defined locally in both space and time. This provides an ideal complement to an eddy energy diagnosis.

Some comparisons of eddy energy and wave activity budgets have been given by Chang and Orlanski (1994) and Chang (2001), using the wave activity of Plumb (1986). Thorncroft et al. (1993) and Magnusdottir and Haynes (1996) employed small- and large-amplitude wave activities, respectively, to interpret the evolution of idealized baroclinic-wave life cycles. Danielson et al. (2006, hereafter Part I) consider a good example of downstream baroclinic development (identified by its eddy energy evolution) and examine the impact of upstream perturbations. In this part, we focus on whether a wave activity diagnosis confirms the interpretation that downstream development is relevant. We take advantage of the properties of the TN01 wave activity to quantitatively compare wave propagation in terms of group velocity and to evaluate conventional methods of isolating a wave packet (Bloomfield 1976; Zimin et al. 2003). The next section provides a description of the two diagnostics. Local eddy energy and wave activity evolutions and a comparison in terms of group velocity are given in section 3. This is followed by a discussion of nonlinear aspects of this event in section 4 and a summary of results in section 5.

2. Wave propagation diagnostics

We begin by identifying the basic elements of idealized upper-level wave packet propagation. Figure 1, adapted from Chang (1993), depicts a wave train of linear potential vorticity (PV) anomalies (open ovals). Cyclonic and anticyclonic anomalies correspond to troughs and ridges, respectively. These PV anomalies do not influence each other directly, but since their influence radii overlap, there are eddy kinetic energy centers in fixed positions between the PV anomalies (shaded ovals). The interaction between these energy centers is defined primarily by a dispersive flux of eddy energy. This ageostrophic geopotential flux (closed arrows) is useful for diagnosing the dynamical depen-

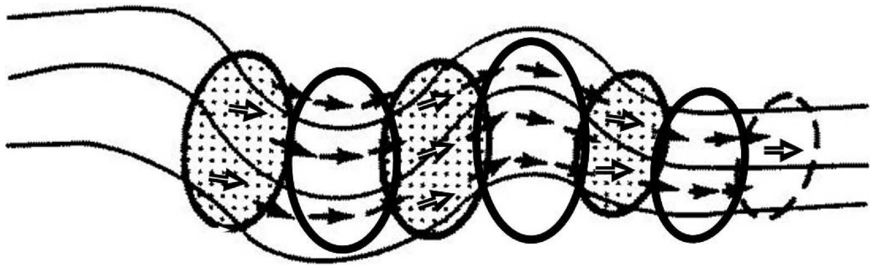

FIG. 1. Eddy energy and wave activity fluxes in an idealized wave train of troughs and ridges. Note that we assume a perspective moving at the phase speed of the PV anomalies. Upper-level geopotential height is contoured. Open ovals correspond to the cyclonic potential vorticity anomalies of troughs and the anticyclonic potential vorticity anomalies of ridges. Shaded ovals correspond to eddy kinetic energy centers. Closed arrows represent ageostrophic geopotential fluxes, and open arrows represent the momentum fluxes described by TN01 (see text). This figure is adapted from Chang (1993).

dence between eddy energy centers (Orlanski and Katzfey 1991).

Like eddy energy, the ageostrophic geopotential flux is strongly dependent on wave phase. This flux is generally strongest along trough and ridge axes. Because the wave activity of TN01 is a weighted combination of eddy energy and eddy enstrophy, this phase dependence is removed and the full extent of the wave packet can be identified. TN01 further show that the corresponding wave activity flux is phase independent. It includes a contribution along ridges and troughs that corresponds to the ageostrophic geopotential flux, and also a contribution in regions of the eddy energy centers (open arrows). The physical interpretation of the latter contribution is given by TN01 as a westward transport of westerly momentum (i.e., a momentum transport opposite to the propagation of wave activity shown in Fig. 1).

A comparison of the two diagnoses can be simplified by defining both wave activity and eddy energy with respect to the same basic state. Here, we employ a 30-day time mean centered on the onset of surface deepening of the eastern cyclone. Prior studies indicate that deviations from a 30-day time mean are generally sufficient to capture the spectrum of wave frequencies relevant to downstream development (Chang and Yu 1999). Denoting eddy variables by the lower case and 30-day mean variables by an overbar, the horizontal wind velocity, three-dimensional wind velocity, geopotential height, and potential temperature are

$$\begin{aligned}
\mathbf{V} &= [U, V, 0]^{\mathrm{T}} = \overline{\mathbf{V}} + \mathbf{v},\\
\mathbf{U} &= [U, V, \omega]^{\mathrm{T}} = \overline{\mathbf{U}} + \mathbf{u},\\
\Phi &= \overline{\Phi} + \phi = \Phi_r(p) + \overline{\Phi_d} + \phi, \quad \text{and}\\
\Theta &= \overline{\Theta} + \theta = \Theta_r(p) + \overline{\Theta_d} + \theta,
\end{aligned} \tag{2}$$

respectively (superscript T denotes a vector transpose). Also, the time-mean geopotential height and potential temperature are separated into a reference state (based on the U.S. standard atmospheric profile) that varies only in the vertical (Φ_r and Θ_r) and spatially varying deviations from this reference state ($\overline{\Phi}_d$ and $\overline{\Theta}_d$). These fields are derived from the global National Centers for Environmental Prediction reanalyses (Kalnay et al. 1996) on 17 pressure levels and at 6-hourly intervals.

a. Eddy energy

Although the role of downstream development in intensifying cyclones can be described solely in the context of the eddy kinetic energy budget (Orlanski and Sheldon 1995), a comparison with wave activity is facilitated by specifying both the eddy kinetic K_e and eddy available potential energy A_e budgets. Following Orlanski and Katzfey (1991),

$$K_e = \frac{u^2}{2} + \frac{v^2}{2}, \tag{3}$$

$$A_e = -\frac{\theta^2}{2}\frac{R}{p}\left(\frac{p}{p_o}\right)^{\kappa}\left(\frac{d\Theta_r}{dp}\right)^{-1}, \tag{4}$$

where R is the gas constant, p is pressure, p_o is reference pressure, and κ is the gas constant to specific heat ratio. The corresponding budgets are

$$\frac{d}{dt}K_e = -\mathbf{v}\cdot\boldsymbol{\nabla}_p\phi - \mathbf{v}\cdot(\mathbf{u}\cdot\boldsymbol{\nabla}\overline{\mathbf{V}}) + \mathbf{v}\cdot\overline{(\mathbf{u}\cdot\boldsymbol{\nabla}\mathbf{v})} + R_\kappa \tag{5}$$

and

$$\frac{d}{dt}A_e = +\alpha\omega + (\theta\mathbf{u}\cdot\boldsymbol{\nabla}\overline{\Theta_d} + \theta\overline{\mathbf{u}\cdot\boldsymbol{\nabla}\theta})\frac{R}{p} \times \left(\frac{p}{p_o}\right)^{\kappa}\left(\frac{d\Theta_r}{dp}\right)^{-1} + R_A, \tag{6}$$

respectively, with ∇ being the three-dimensional and ∇_p the horizontal gradient operators. Numerical computations are made by centered differences, with pressure-level terms interpolated linearly in pressure to vertical midlevels following their computation at original data levels, and vertical derivatives solved directly at midlevels.

The terms on the lhs of (5) and (6) are the Lagrangian tendencies ($d/dt = \partial/\partial t + \mathbf{U} \cdot \nabla$). The first two terms on the rhs ($\mathbf{v} \cdot \nabla_p \phi$ and $\alpha\omega$) are the generation of K_e and the baroclinic conversion of A_e, respectively. (By convention, we refer to *negative* $\alpha\omega$ as *positive* baroclinic conversion because when $\alpha\omega < 0$, A_e is converted to K_e.) The relationship between these two terms is discussed below. The next two terms are the Reynolds' stress and the conversion from mean to eddy available potential energy. The latter is a function of the horizontal gradient of mean potential temperature $\nabla_p \overline{\Theta}_d$, which is proportional to baroclinicity (Hoskins 1990). This pair of terms is related to a corresponding pair of terms in the mean energy budgets. Hence, they are interpreted as contributing to mean-eddy energy transfer in the local sense (Orlanski and Katzfey 1991). The second to last terms are the correlation conversion terms. These are also conversions between different forms of energy, though they are zero in an averaged sense. The final terms (R_κ and R_A) represent frictional dissipation and diabatic processes, respectively. They are calculated as budget residuals and thus include energy transfers at the scale of the analysis grid and any discretization errors.

The relative importance of a given process, such as downstream development, can be difficult to gauge using (5) and (6). This is because the flux and conversion terms (i.e., the rhs terms, except for the residuals) are not necessarily unique. For example, the role of mean-flow deformation in eddy energy growth is most easily understood by reformulating the Reynolds' stress term, following Lackmann et al. (1999). If Reynolds' stresses are locally negligible but the contribution by deformation is not, the importance of mean-eddy energy conversion may be unclear. If no particular physical interpretation is assigned, moreover, flux and conversion terms can be expressed in an unlimited number of ways. Broad ambiguities of the energy budget system are given by Plumb (1983) in the context of zonally averaged flows. Below, we indicate that the unaveraged flux and conversion terms of (5) and (6) are not entirely ambiguous, however, because the eddy flux terms can be constrained to yield a measure of group velocity (Chang and Orlanski 1994).

Kinetic energy generation $\mathbf{v} \cdot \nabla_p \phi$ and baroclinic conversion $\alpha\omega$ represent a conversion between A_e and K_e. For a nondivergent time-mean flow, they are related by

$$-\mathbf{v} \cdot \nabla_p \phi = -\alpha\omega - \nabla_p \cdot (\phi \mathbf{v})_a - \frac{\partial}{\partial p}(\phi\omega). \tag{7}$$

The last two terms on the rhs represent the divergence of a radiative energy flux (Orlanski and Katzfey 1991). The horizontal component, $(\phi\mathbf{v})_a$, is the ageostrophic geopotential flux and is defined by Orlanski and Sheldon (1993) as

$$(\phi\mathbf{v})_a = \phi\mathbf{v} - \hat{\mathbf{k}} \times \nabla \frac{\phi^2}{2f}, \tag{8}$$

where $\hat{\mathbf{k}}$ is a unit vertical vector. This is the eddy geopotential flux with a nondivergent (essentially geostrophic) part omitted. For an idealized baroclinic wave train, this flux is represented in Fig. 1 by closed arrows. To highlight the horizontal component of energy propagation, terms in (3)–(8) are vertically integrated. This results in a simplification of the local budgets insofar as the dominant lateral (i.e., downstream) interactions between eddy kinetic energy centers are emphasized and all vertical flux divergence terms become quite small. Integrals are performed from the surface to 100 hPa (the upper limit of the vertical velocity data), normalized by the constant of gravity to obtain units of J $\mathrm{m^{-2}}$ for energy and W $\mathrm{m^{-2}}$ for the budget terms.

b. *Wave activity*

The wave activity of TN01 is derived for small-amplitude quasigeostrophic (QG) eddies. Its derivation assumes only slow, large-scale variations of an unforced basic state and of the time-mean propagation of the eddies. A conservation equation can be expressed in the form (1), or

$$\frac{\partial M}{\partial t} + \nabla \cdot \mathbf{W} = D, \tag{9}$$

where $\mathbf{W}$ is the flux of wave activity, and D represents nonconservative (diabatic or frictional) forcing. The wave activity M is the sum of an eddy potential enstrophy (i.e., half the square of eddy quasigeostrophic PV, hereafter QGPV, which is defined below) and eddy energy, both of which are normalized by basic-state variables.

Takaya and Nakamura (1997) and TN01 find that the combination of energy and enstrophy leads to a wave activity pseudomomentum that is independent of wave phase. For an idealized sinusoidal wave, eddy energy and eddy enstrophy would then be proportional to sine squared and cosine squared of such a wave. [By comparison, pseudoenergy can be defined as the difference between normalized energy and enstrophy, but as with energy or enstrophy alone, this is strongly dependent on wave phase (TN01).] Therefore, the entire wave packet is revealed by their definition, and the lack of phase dependence allows a local wave activity to be defined. Using pressure and spherical coordinates (where λ is longitude and φ is latitude), it takes the form

$$M = \frac{\cos\varphi}{2}\left(\frac{q^2}{2|\nabla_p \overline{Q}|} + \frac{e_g}{|\overline{\mathbf{V}}_g| - |\overline{\mathbf{C}}_\upsilon|}\right), \qquad (10)$$

where $q(\overline{Q})$ is the eddy (mean) QGPV, e_g is the eddy QG energy (both kinetic and potential), $\overline{\mathbf{V}}_g$ is the mean geostrophic wind velocity, and $\overline{\mathbf{C}}_\upsilon$ defines the time-mean velocity of the eddies in the direction of the mean geostrophic flow. (Note that M is well defined only where $|\nabla_p \overline{Q}| > 0$ and $|\overline{\mathbf{V}}_g| > |\overline{\mathbf{C}}_\upsilon|$.)

The quantities in (10) can be written in terms of the geostrophic streamfunction $\Psi = \Phi/f$, or equivalently, the geopotential Φ and potential temperature Θ. We can then define the geostrophic flow as

$$\mathbf{V}_g = [U_g, V_g]^{\mathrm{T}} = \left[-\frac{1}{a}\frac{\partial \Phi/f}{\partial \varphi}, \frac{1}{a\cos\varphi}\frac{\partial \Phi/f}{\partial \lambda}\right]^{\mathrm{T}}, \qquad (11)$$

where a is the mean radius of the earth, and the time mean and eddy flows $\mathbf{V}_g = \overline{\mathbf{V}}_g + \mathbf{v}_g$ are similarly defined. The mean and eddy QGPV are

$$\overline{Q} = f + \frac{1}{a\cos\varphi}\left(\frac{\partial \overline{V}_g}{\partial \lambda} - \frac{\partial \overline{U}_g \cos\varphi}{\partial \varphi}\right) + f\frac{\partial}{\partial p}\left(\frac{\overline{\Theta}_d}{d\Theta_r/dp}\right) \qquad (12)$$

and

$$q = \frac{1}{a\cos\varphi}\left(\frac{\partial \upsilon_g}{\partial \lambda} - \frac{\partial u_g \cos\varphi}{\partial \varphi}\right) + f\frac{\partial}{\partial p}\left(\frac{\theta}{d\Theta_r/dp}\right), \qquad (13)$$

respectively. Finally, the eddy QG energy density is

$$e_g = \frac{u_g^2}{2} + \frac{\upsilon_g^2}{2} - \frac{\theta^2}{2}\frac{R}{p}\left(\frac{p}{p_o}\right)^\kappa \left(\frac{d\Theta_r}{dp}\right)^{-1}. \qquad (14)$$

Note that e_g differs from $E_e = K_e + A_e$ only in that the geostrophic winds are used here.

Given the preceding definitions, the wave activity flux of TN01 can be written

$$\mathbf{W} = \frac{\cos\varphi}{2|\overline{\mathbf{V}}_g|}\begin{bmatrix} \overline{U}_g\left(\upsilon_g^2 - \frac{\phi}{f}\frac{1}{a\cos\varphi}\frac{\partial \upsilon_g}{\partial \lambda}\right) + \overline{V}_g\left(-u_g\upsilon_g + \frac{\phi}{f}\frac{1}{a\cos\varphi}\frac{\partial u_g}{\partial \lambda}\right) \\ \overline{U}_g\left(-u_g\upsilon_g - \frac{\phi}{f}\frac{1}{a}\frac{\partial \upsilon_g}{\partial \varphi}\right) + \overline{V}_g\left(u_g^2 + \frac{\phi}{f}\frac{1}{a}\frac{\partial u_g}{\partial \varphi}\right) \\ \frac{f}{d\Theta_r/dp}\left(\overline{U}_g\upsilon_g\theta - \overline{U}_g\phi\frac{1}{a\cos\varphi}\frac{\partial \theta/f}{\partial \lambda} - \overline{V}_g u_g\theta - \overline{V}_g\phi\frac{1}{a}\frac{\partial \theta/f}{\partial \varphi}\right) \end{bmatrix} + M\overline{\mathbf{C}}_\upsilon. \qquad (15)$$

The first term on the rhs is denoted $\mathbf{W}_s$ and represents the flux for stationary Rossby waves (Takaya and Nakamura 1997). For nonstationary waves on a zonal-mean flow ($\overline{V}_g \approx 0$), each component of $\mathbf{W}_s$ is dominated by its first two terms, and TN01 provide an interpretation of the second terms as an ageostrophic geopotential flux normalized by $|\overline{\mathbf{V}}_g| - |\overline{\mathbf{C}}_\upsilon|$. Hence, as with the eddy energy flux, these terms dominate *along* ridges and troughs, but for a typical mean shear, they will not increase with height as quickly. (Note that $\overline{\mathbf{C}}_\upsilon$ is constant in the vertical.) Also, because the first terms in each component of (15) dominate *between* ridges and troughs, wave activity flux is also independent of wave phase. This component of wave activity flux is represented in Fig. 1 by open arrows.

TN01 define $\overline{\mathbf{C}}_\upsilon$ as the component of the mean phase velocity of the eddies along the mean flow. They calculate this by connecting the locations of maximum positive and negative time-lagged correlations in high-pass-filtered 250-hPa geopotential height fluctuations, and taking the component of this velocity in the direction of the 250-hPa time-mean flow. We employ the same method using a 30-day time series of the eddy meridional wind at 300 hPa (Chang and Yu 1999). A comparison of the resulting velocity (Fig. 2) with the tracks of the individual western and eastern troughs (which move at about 15 m s^{-1}), suggests that their movement is roughly similar to the mean 300-hPa phase velocity where the mean flow is strong.

To compare with the evolution of eddy energy, we vertically average the wave activity and its fluxes, just as eddy energy is vertically integrated (i.e., we normalize by the column mass per unit area). However, wave activity is undefined where the mean phase speed $|\overline{\mathbf{C}}_\upsilon|$ is greater than the mean flow $|\overline{\mathbf{V}}_g|$. Since the mean flow varies in the vertical (and mean phase speed does not), wave activity tends to be defined mainly at upper levels. Defined values tend to be sparse everywhere below 600 hPa for our evolution. The resulting vertical averages of wave activity and its flux are undefined within the

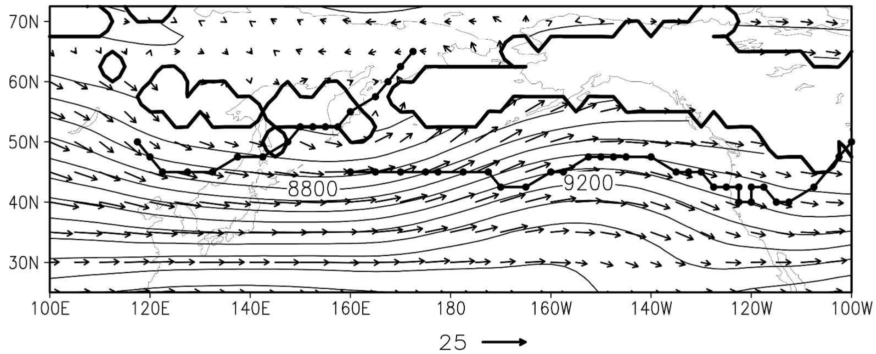

FIG. 2. The component of the mean phase velocity of the eddies $\overline{\mathbf{C}}_v$ in the direction of the 300-hPa mean flow $\overline{\mathbf{V}}_g$ and the 300-hPa mean height (at 100-m intervals). Fields are masked where wave activity is undefined (see text). Also shown are the tracks of the western and eastern North Pacific troughs at 6-h intervals (thick lines with closed circles), beginning at 0000 UTC 8 Mar 1977.

masked region in Fig. 2 (where $|\overline{\mathbf{V}}_g| - |\overline{\mathbf{C}}_v| < 2$ m s^{-1}). Also, defined values on the border of these regions are mainly representative of tropopause levels (where $|\overline{\mathbf{V}}_g|$ is large). This yields units of m s^{-1} for wave activity and m s^{-2} for the budget terms.

c. Group velocity

A quantitative comparison between the propagation of eddy energy and wave activity is available in terms of group velocity $\mathbf{C}_g$. For eddy energy, we define this as

$$\mathbf{C}_{ge} = \frac{\int\int \overline{\mathbf{V}}E_e + (\phi\mathbf{v})_a \, dp \, dA}{\int\int E_e \, dp \, dA}, \tag{16}$$

following Orlanski and Chang (1993). Here, E_e is the eddy energy density ($E_e = K_e + A_e$). This is not the only possible expression of group velocity in terms of eddy energy, but one that seems appropriate because the wave activity of TN01 is also based on the assumption of a linear flow (cf. Pedlosky 1987, section 6). For idealized *nonlinear* flows, the full wind, rather than the mean wind, advects eddy energy in the numerator of (16) (Orlanski and Chang 1993). The nonlinear estimate of group velocity is generally faster than the linear estimate (see section 4). To remove the dependence of $\mathbf{C}_{ge}$ on wave phase, integration is performed over an area defined by an eddy energy center (Orlanski and Katzfey 1991), with a cutoff contour of 3 MJ m^{-2}. We note that $\mathbf{C}_{ge}$ is not very sensitive to the precise value of the cutoff.

TN01 show that group velocity is defined as the wave activity flux $\mathbf{W}$ divided by wave activity M. The quantity corresponding to $\mathbf{C}_{ge}$ in terms of wave activity is thus

$$\mathbf{C}_{gw} = \frac{\int\int \mathbf{W} \, dp \, dA}{\int\int M \, dp \, dA}. \tag{17}$$

Areal integration is performed over a wave activity center using a cutoff contour of 30 m s^{-1} (and here also, the result is not sensitive to the precise value). Strictly speaking, it is acceptable to define a *local* group velocity using the wave activity of TN01 but not using eddy energy because of its dependence on wave phase. To compare with $\mathbf{C}_{ge}$, the regions of integration are chosen to be as similar as possible. Both regions are shown in section 4 to demonstrate that they are well defined.

The group velocities defined by $\mathbf{C}_{gw}$ and $\mathbf{C}_{ge}$ provide measures of the speed at which the wave packet or the envelope of eddy energy is moving downstream. However, to estimate this directly, we will find a phase-independent definition of wave activity to be useful. To obtain a third estimate of group velocity, we will simply follow the contiguous (phase independent) wave activity center.

3. Linear diagnoses

Before comparing eddy energy and wave activity evolutions, it is instructive to characterize the dynamic tropopause evolution of the two North Pacific cyclones involved (see Part I for a discussion of the surface features). We take the dynamic tropopause to be the 2-PVU surface (PVU, or PV unit, is defined as 10^{-6} m^2 s^{-1} K kg^{-1}). The western trough, depicted as an equatorward and surfaceward extrusion of cold potential temperature on the dynamic tropopause, is over Mongolia at 0000 UTC 8 March (Fig. 3a). At this time,

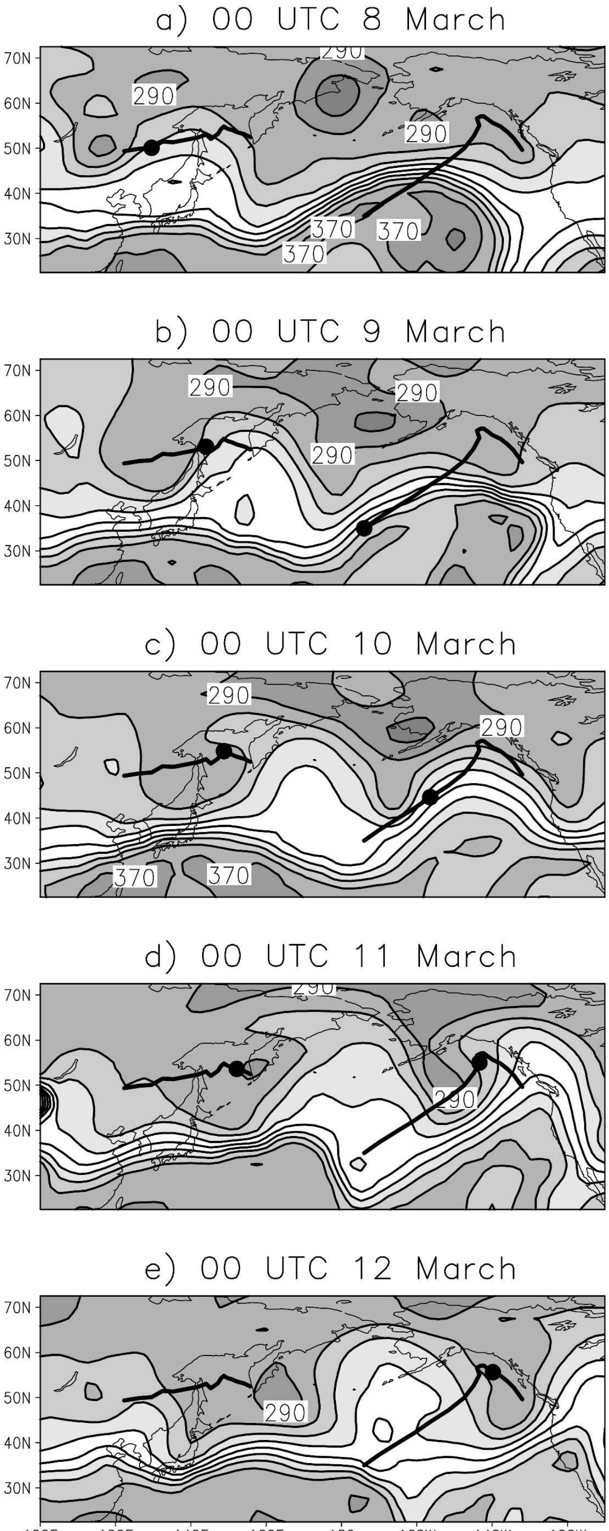

FIG. 3. Evolution of tropopause potential temperature at 0000 UTC (a) 8 Mar, (b) 9 Mar, (c) 10 Mar, (d) 11 Mar, and (e) 12 Mar 1977. Contour intervals are 10 K with values between 320 and 340 K unshaded. As in subsequent figures, the tracks of the western and eastern surface cyclones are included with a dot to indicate the current position.

the eastern trough is approaching the date line and there is a prominent ridge and split flow between the two troughs. Another feature of interest is a subtropical trough over the North American coast. This feature wraps up anticyclonically and then is not apparent in the upper-level analyses after 9 March (Figs. 3b,c).

Both western and eastern troughs can be characterized as amplifying and wrapping up cyclonically (Fig. 3d; LC2-type wave breaking, using the nomenclature of Thorncroft et al. 1993). Nearby contours equatorward of about 320 K (including the unshaded regions) remain approximately undular, and we might infer that the large-scale dynamics are predominantly linear. Farther north, the western trough becomes isolated by closed potential temperature contours after about 0000 UTC 10 March, and the eastern trough becomes isolated about one day later. This suggests that strong nonlinearities and trapping of parcels within these vortices occur over relatively large scales (Hakim 2000). Our inference that the evolution of these troughs becomes nonlinear between 10 and 11 March will be relevant in section 4.

a. *Eddy energy diagnosis*

Downstream baroclinic development (Orlanski and Sheldon 1995) provides an idealization of cyclone development in terms of eddy energy. According to this evolution, eddy kinetic energy initially disperses across a preexisting ridge. This triggers energy growth on the upstream side of an incipient trough, followed by baroclinic conversion (descent in relatively cold air in the wake of a growing eastern cyclone). As this energy center matures, it becomes an energy source for another center just downstream of the trough axis, while the energy center upstream of the ridge axis decays. Subsequently, the downstream center is fed by baroclinic conversion as well (ascent in relatively warm air ahead of the eastern cyclone), and may act as a source of eddy energy for further development downstream.

The idealized evolution can be compared with that of the observed western and eastern cyclones in Fig. 4. Eddy energy is found to disperse across the ridge between the two cyclones throughout the period shown. Notably, the upstream source feeding this propagation seems to be baroclinic conversion in warm ascent near the western cyclone. This conversion is seen on 0000 UTC 8 March (Fig. 4f) in association with upward motion near the western cyclone. Baroclinic conversion and ageostrophic geopotential flux divergence characterize the corresponding western energy center, which is shown by a thick contour in Fig. 4a. Energy disperses across the ridge toward a central Pacific energy center (thick contour in Fig. 4b). This central energy center

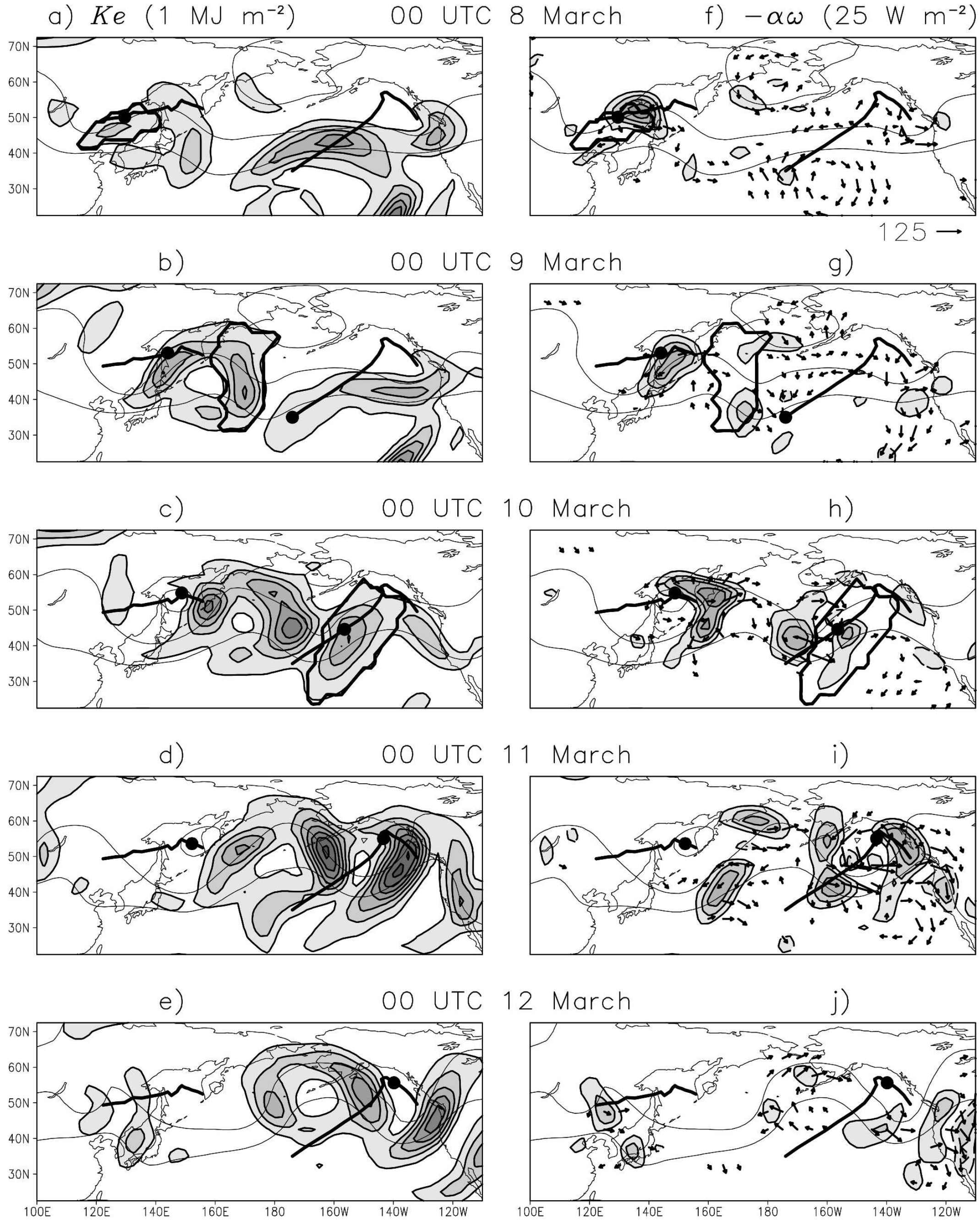

FIG. 4. The evolution of eddy kinetic energy for 0000 UTC 8–12 Mar 1977: vertical integrals of (a)–(e) eddy kinetic energy and (f)–(j) baroclinic conversion and the ageostrophic geopotential flux (vectors less than 30 MW m^{-1} are omitted, and as with subsequent figures, every other vector is shown with a reference vector near the top). Repeated thick contours on the left and right isolate the (a), (f) western, (b), (g) central, and (c), (h) eastern energy centers, for which energy budget terms are shown in Fig. 5 (see text). Contour intervals are 1 MJ m^{-2} for energy and 25 W m^{-2} for baroclinic conversion. Geopotential height at 500 hPa is included (thin contours at 30-dam intervals).

also benefits from baroclinic conversion in the form of cool descent (Fig. 4g), associated with the spinup of the eastern surface cyclone. Subsequently, the growth of an eastern energy center (thick contour in Fig. 4c) is promoted by both eddy energy dispersing across the eastern trough axis and baroclinic conversion in warm ascent near the eastern surface cyclone. Based on the local propagation of eddy energy, not only does down-

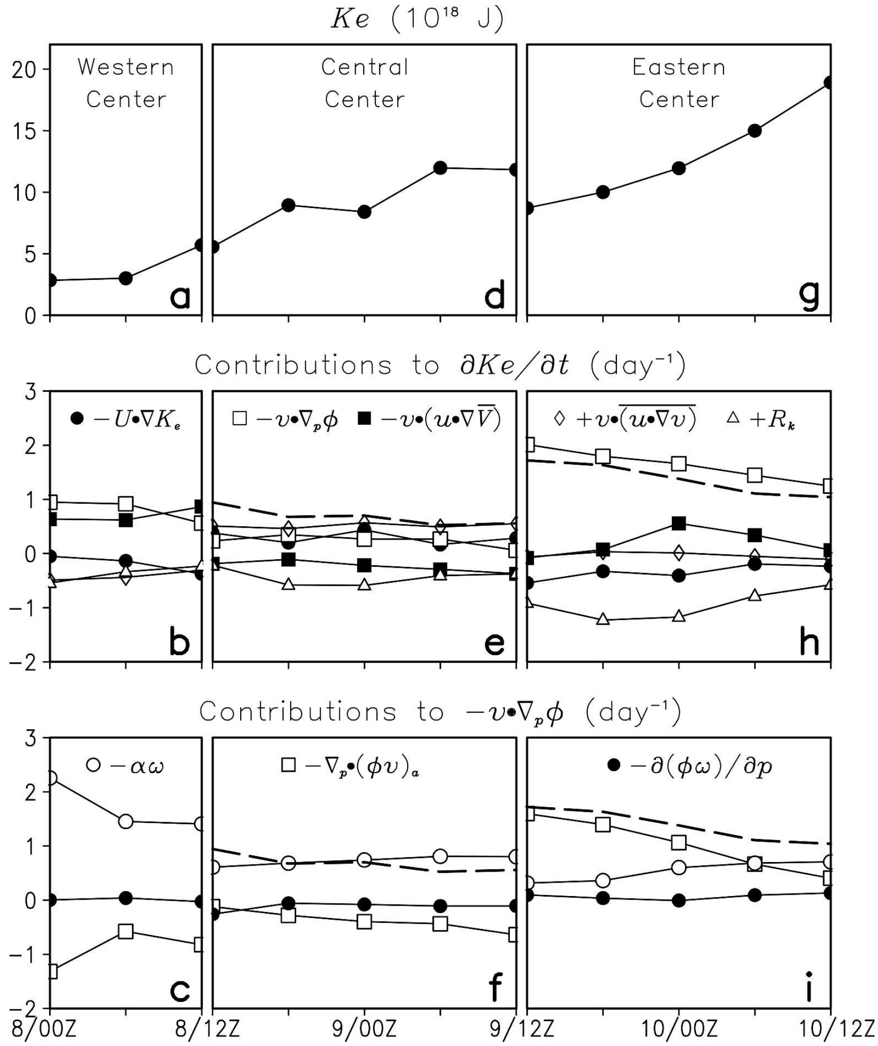

FIG. 5. Eddy kinetic energy budget summaries for the (a)–(c) western energy center between 0000 and 1200 UTC 8 Mar, (d)–(f) central energy center between 1200 UTC 8 and 9 Mar, and (g)–(i) eastern energy center between 1200 UTC 9 and 10 Mar 1977: contributions to (b), (e), (h) the tendency of K_e and to (c), (f), (i) the generation of K_e. The dashed line in (e), (f), (h), and (i) is the positive contribution to the ageostrophic geopotential flux divergence term (see text for a definition of terms). Eddy kinetic energy has units of 10^{18} J, and the budget terms are expressed as growth rates (days^{-1}).

stream development across the North Pacific appear to be relevant to the eastern cyclone, but the earlier growth of eddy energy in the western cyclone does as well.

If we neglect the ambiguity in how some energy budget terms may be defined, the importance of energy propagation from the western cyclone can be emphasized by comparison with the other terms of the eddy kinetic energy budget (5). Figure 5 illustrates the contributions to the growth of the western, central, and eastern energy centers during three periods that are chosen subjectively to highlight the role of downstream energy propagation. Note that budget terms are expressed as growth rates because eddy kinetic energy varies in time and from one center to another.

The intensity of the western energy center during 0000–1200 UTC 8 March is governed primarily by two competing processes: growth by baroclinic conversion and decay by energy propagation (Fig. 5c). [The smaller positive contribution from the Reynolds' stress term is associated with deformation in the mean flow (cf. Lackmann et al. 1999).] During the next 24 h, the central energy center benefits from baroclinic conversion, correlation conversion, and positive advective flux divergence (Figs. 5e,f). Notably, the ageostrophic geopotential flux divergence term does not contribute much to the net growth or decay of this energy center. However, this is because of the contemporaneous positive energy flux divergence from the western center and negative energy flux divergence toward the eastern energy center (Fig. 4g). Other good examples of downstream baroclinic development also show evidence of energy propagation through energy centers such as this one, which might be described as mature (Danielson et al. 2004). We reconcile this with the idealized evolution (Orlanski and Sheldon 1995) by considering separately the positive and negative contributions to the ageostrophic geopotential flux divergence term, where the former is assumed to represent the convergent flux from upstream (see also Orlanski 1994). If this is done, the positive contribution (dashed line in Fig. 5e) is found to be as important as any other to the growth of the central energy center.

Growth of the eastern energy center between 1200 UTC 9–10 March is first by energy propagation from upstream and subsequently by Reynolds' stresses and baroclinic conversion. This is quite consistent with the idealized evolution, and hence, this event seems to represent a good example of downstream baroclinic development. However, it is not evident that we can be conclusive about this without considering all contributions to the energy budget terms whose form we have not constrained by specific physical interpretation. Wave activity budget terms are, by comparison, better constrained.

b. *Wave activity diagnosis*

The phase-dependent sequence of events that characterizes the downstream propagation of eddy energy should essentially be masked by the wave activity of TN01. Of course, the separate energy or enstrophy phases are both available for examination, and the direction of wave activity and eddy energy propagation is expected to correspond well in the vicinity of trough and ridge axes (cf. Orlanski and Chang 1993; TN01). However, to diagnose the dynamical connection between the western and eastern cyclones using wave activity, we propose to show that the western and eastern cyclones are both members of the same contiguous wave packet that exists in the west during the development of the western cyclone, and later in the east during the development of the eastern cyclone. From this point of view, it seems reasonable to expect that the eastern cyclone is sensitive to an earlier amplification of its wave packet by the western cyclone.

The evolution of wave activity between the western and eastern cyclones is shown in Fig. 6 and essentially

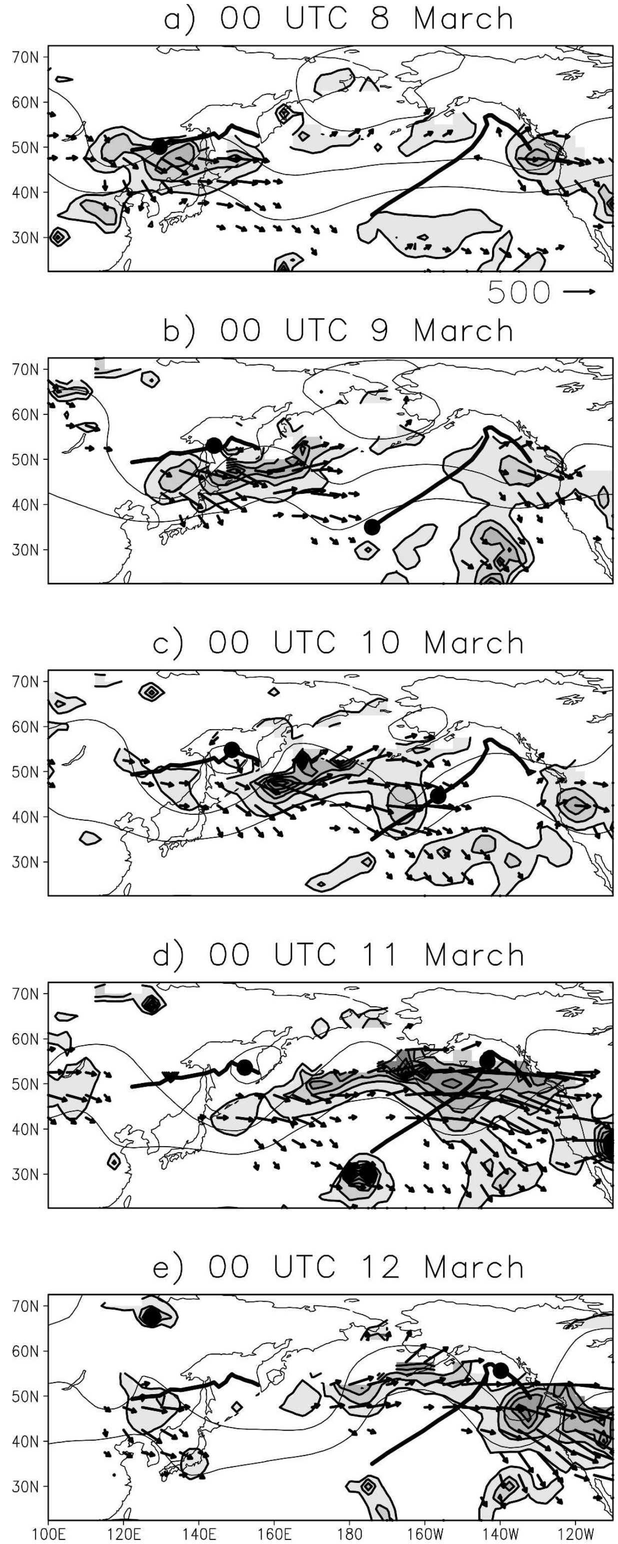

FIG. 6. The evolution of wave activity for 0000 UTC 8–12 Mar 1977. As in Figs. 4a–e, but for the vertical average of wave activity and the stationary wave activity flux $\mathbf{W}_s$ relative to the mean phase speed of the upper-level waves. The wave activity contour interval is 30 m s^{-1}.

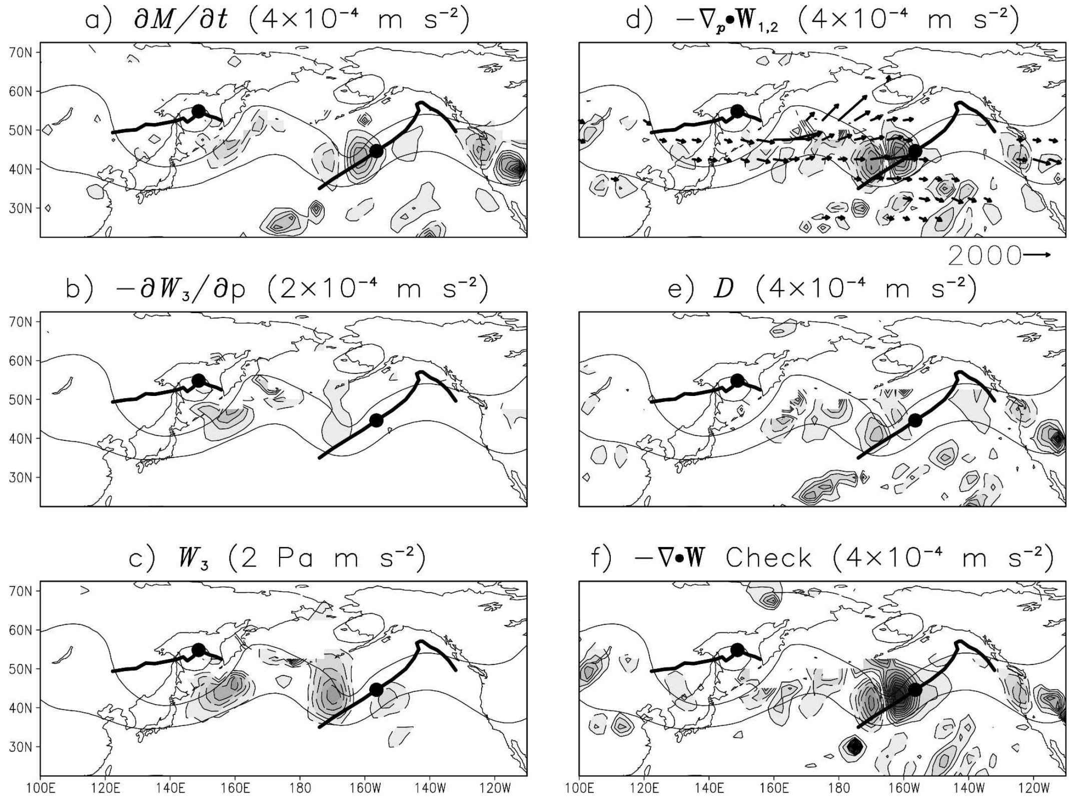

FIG. 7. The wave activity budget at 0000 UTC 10 Mar 1977: Vertical averages of (a) the tendency, (b) vertical, and (d) horizontal components of the flux divergence, and (e) the budget residual. Wave activity fluxes greater than 400 $m^2 s^{-2}$ are included in (d). Also shown are (c) the vertical flux (dashed contours are negative and indicate upward fluxes) and (f) a flux divergence consistency check (see text). The contour intervals are 4×10^{-4} m s^{-2} (half this for vertical flux divergence) and 2 Pa m s^{-2} for the budget terms and the vertical flux, respectively.

confirms that both cyclones are members of the same wave packet. This feature is collocated with the western cyclone at 0000 UTC 8 March (Fig. 6a), as well as with *both* the western and upstream energy centers (Fig. 4a). Wave activity fluxes relative to the phase speed of upper-level waves ($\mathbf{W}_s$) are directed predominantly downstream (for clarity, fluxes less than 100 $m^2 s^{-2}$ are masked). As expected, they are consistent with the direction of the ageostrophic geopotential fluxes at trough and ridge axes, but are directed downstream throughout the wave packet.

During the next three days (Figs. 6b–d), a lengthening of the wave packet is explained mainly by its relative fluxes, or at least those directed downstream at the leading edge. (In the absence of diabatic and frictional forcing, the relative wave activity fluxes simply expand the wave packet where they are directed away from it, and contract the wave packet where they are directed toward it.) The local maximum in wave activity shifts to the eastern trough by 0000 UTC 11 March (Fig. 6d), when the eastern cyclone is most intense. The wave packet then remains zonally extensive and the downstream fluxes intensify. The packet eventually begins to merge with another near the North American west coast, although prior to 11 March these two centers are distinct.

A single wave packet contains both the western and eastern cyclones, although local maxima in wave activity are also associated with each surface cyclone. This is particularly apparent at 0000 UTC 10 March (Fig. 6c). To identify local sources of wave activity, the corresponding budget (9) of the lengthening wave packet is shown in Fig. 7. (Note that vertically averaged terms are employed to be consistent with our diagnosis using eddy energy, and these represent the layer above approximately 600 hPa here). As the wave packet elongates, the Eulerian tendency is positive at the leading edge and only slightly negative at the trailing edge of the wave packet (Fig. 7a). The dominant contribution to the tendency is a horizontal flux divergence [$-\nabla_p \cdot W_{1,2}$, where the individual flux components are $\mathbf{W} = (W_1, W_2, W_3)^T$; Fig. 7d].

The wave packet elongation is primarily governed by a downstream flux of wave activity, but where the wave packet is collocated with a surface cyclone, an adiabatic source of wave activity occurs by an upward flux from the lower troposphere (Fig. 7c). Hence, the persistence of the wave packet in the west, and part of its eastern growth, can be attributed to an upward wave activity propagation and positive flux divergence ($-\partial W_3/\partial p$; Fig. 7b). This divergence and the baroclinic conversion term (Fig. 4h) seem quite consistent with each other, as they are both strongest near the western cyclone.

The budget residual (Fig. 7e) does not suggest a strong relationship with latent heat release, which we might infer to be a primary diabatic forcing of wave activity above the boundary layer. Particularly near the western cyclone, however, latent heat release may occur outside the region where it can be diagnosed (cf. Fig. 2 and baroclinic conversion in Fig. 4h, which is presumably collocated with latent heat release; see also a discussion of precipitation in Part I). Even where wave activity is well defined, however, the budget residual is generally not a practical means of diagnosing diabatic forcing (TN01). This is owing to assumptions in the derivation of (9), such as the basic state is approximately unforced and slowly varying. The basic-state assumption can be checked by recalculating the wave activity flux divergence term, following TN01 [cf. their Eq. (39)]. The result (Fig. 7f) is qualitatively similar to the horizontal flux divergence term (Fig. 7d) at 0000 UTC 10 March, though it is somewhat more similar before 10 March and slightly less so afterward (not shown).

The overall impression is thus of two local sources of wave activity in the western and central North Pacific. These feed a single wave packet that lengthens as it moves downstream, with the local tendency of the packet being dominated by horizontal wave activity fluxes. A similar result is given by Chang (2001), who examines a group of Southern Hemisphere wave packets that are maintained by horizontal fluxes at the leading edge, while vertical fluxes feed the wave packet upstream. [We note that Chang (2001) employs the conservation equation of Plumb (1986), which shares some terms in common with TN01, although the former also requires time averaging to be conserved.] A correspondence between diagnoses of wave activity and eddy energy is evident in Chang (2001) and in our diagnoses of 8–13 March. This provides the impetus for a more direct comparison in terms of group velocity.

c. *Group-velocity comparison*

The propagation of wave activity and eddy energy should essentially be the same for plane waves that are unforced and nearly monochromatic (cf. Longuet-Higgins 1964). Although these approximations are obviously too strict for the case considered here, it is nonetheless of interest to compare the two estimates of wave propagation, $\mathbf{C}_{gw}$ and $\mathbf{C}_{ge}$. These are shown on the right in Fig. 8. The regions over which the fluxes are integrated are defined by the bold contours in the eddy energy (Figs. 8a–f) and wave activity (Figs. 8g–l) evolutions. Where the contiguous wave packet extends over multiple energy centers, all such centers are included within the eddy energy integration domain.

The group velocities agree reasonably well during this 5-day period. A time average of the zonal component yields 16 m s^{-1} for wave activity and 22 m s^{-1} for eddy energy. The agreement is clearly best, both in speed and direction, during 8–10 March (Figs. 8m–o), whereas during 11–12 March the downstream transport of eddy energy appears to be faster. Recalling the dynamic tropopause evolution of section 3, which indicates that the western (eastern) trough exhibits a nonlinear evolution beginning at about 0000 UTC 10 March (11 March), we suggest that the early stage is most relevant for this comparison. In other words, the agreement in group velocities between 8 and 10 March is because of the more linear evolution of the wave packet as it moves across the North Pacific during this initial period. Another measure of group velocity can be made using the center of the phase-independent wave packet itself, which moves about 120° longitude over 5 days at an average speed of 22 m s^{-1} (at 45°N). Although the speed at which wave packets cross the North Pacific varies from case to case (Chang and Yu 1999), if typical speeds are taken to be about 20–30 m s^{-1} then our estimates indicate slow propagation.

The TN01 wave activity is phase invariant and thus affords a local perspective on the variation of group velocity within the evolving wave packet. Previous experiments by Chang and Orlanski (1994) have examined the propagation of linear wave packets in idealized baroclinic flows. They found that at the leading edge of a wave packet, about 70% of the zonal component of group velocity is owing to advection. The rest is owing to dispersion. We revisit the issue here using wave activity. Local contributions to the group velocity $\mathbf{C}_{gw}$ are shown in Figs. 9e,h as a function of length along the North Pacific wave packet. These Hovmöller diagrams are obtained by averaging in latitude over the regions shown in Fig. 8. Local contributions to $\mathbf{C}_{ge}$ are also shown for reference (Figs. 9a,b,d,g). These contain variations that tend to be in phase with ridges and troughs, which propagate upstream relative to the wave packet. The energy contributions are thus unrepresentative of local group velocity unless averaging in longitude is also performed (Figs. 9c,f,i).

The maximum zonal propagation of wave activity is

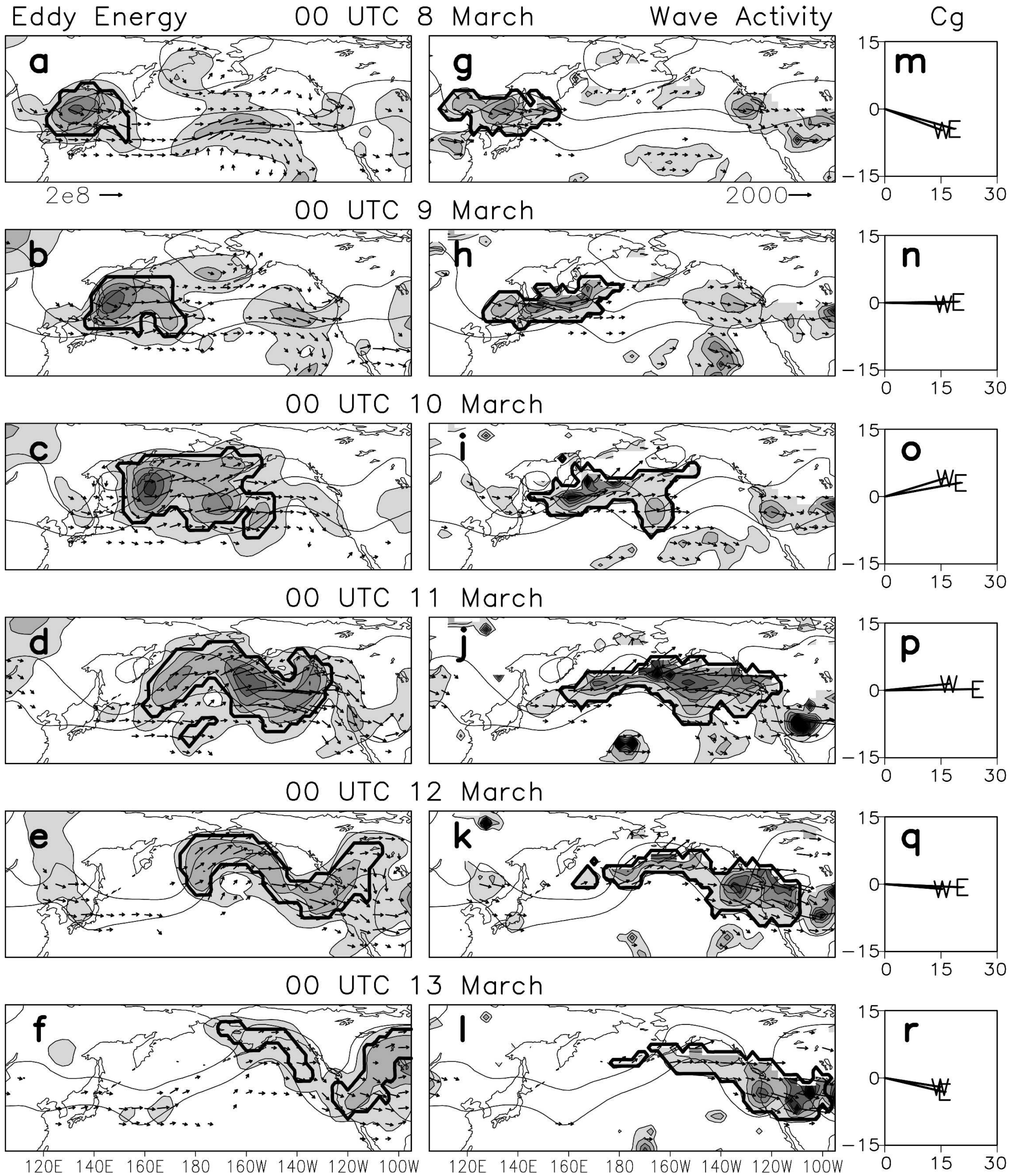

FIG. 8. Comparison of eddy energy and wave activity group velocities for the regions indicated by thick contours in (a)–(l). Vertical integrals of (a)–(f) eddy energy and energy fluxes. Vertical averages of (g)–(l) wave activity and wave activity fluxes. (m)–(r) Group velocities of eddy energy E and wave activity W. Contour intervals are 2 MJ m^{-2} for eddy energy, 30 m s^{-1} for wave activity, and group velocity has units of m s^{-1}. Eddy energy fluxes less than 40 MW m^{-1} and wave activity fluxes less than 400 m^2 s^{-2} are masked. The geographic region shown is from 24° to 72°N.

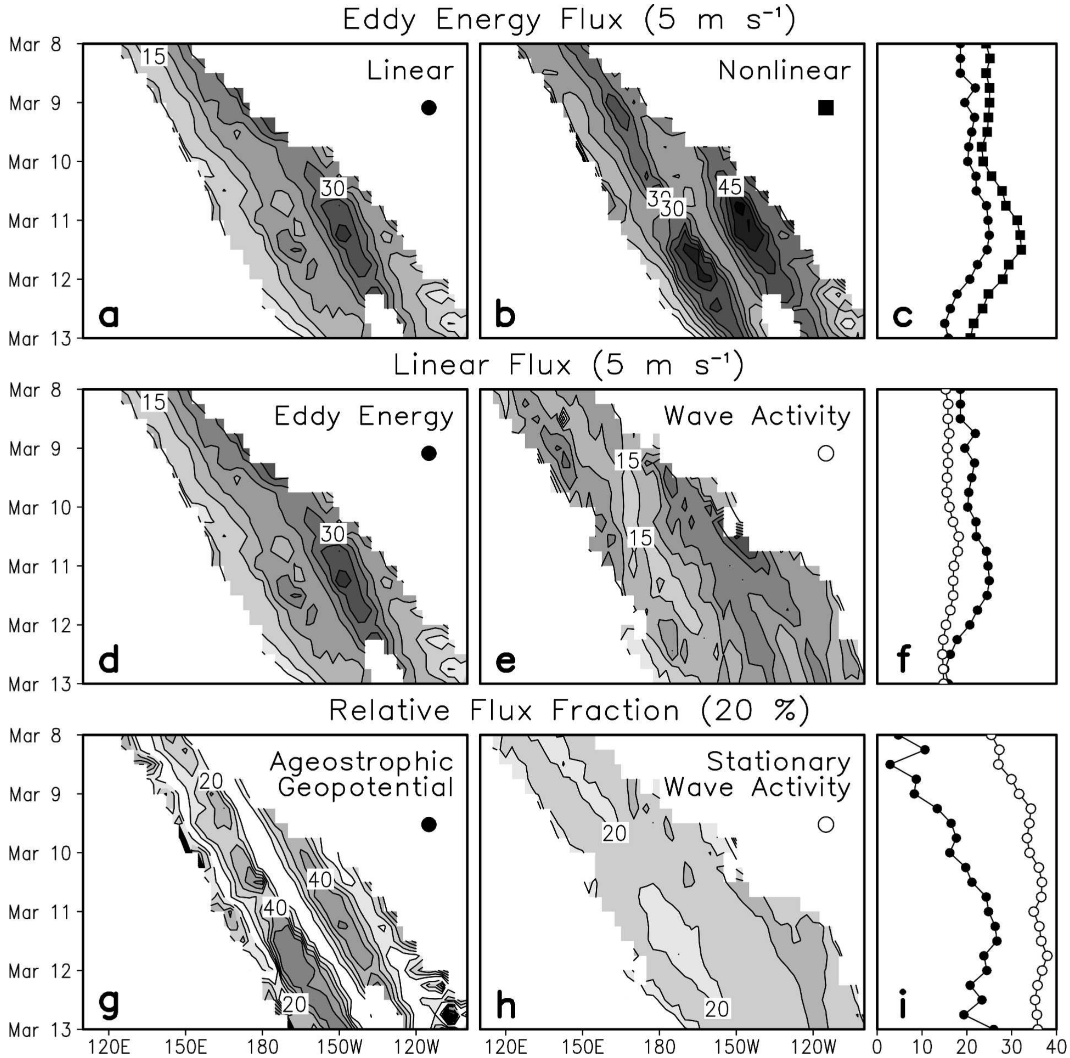

FIG. 9. Contributions to the component of group velocity in the zonal direction for 8–13 Mar 1977, as a function of time and distance along the wave packet: (a), (b) The flux of eddy energy according to linear (filled circle on rhs) and nonlinear (filled square) definitions (see text). (d), (e) Linear estimates of the flux of eddy energy (filled circle on rhs) and wave activity (open circle). (g), (h) The ageostrophic geopotential flux (filled circle on rhs) and the stationary wave activity flux (open circle), expressed as a fraction of their total linear flux. Shown on the right are (c), (f), (i) averages over both latitude and longitude within the regions indicated by bold contours in Fig. 8. Units (contour intervals) are (5) m s^{-1} for (a)–(f) and 20% for (g)–(i). Note that (a) is duplicated in (d).

about 35 m s^{-1} and occurs at the leading edge of the wave packet between 10 and 11 March (Fig. 9e). Group speed is also relatively strong along the trailing edge, and this contrasts with the weak contributions that are resolved using eddy energy. The difference is related to the upstream component of the ageostrophic geopotential flux (Fig. 9g) that is generally resolved at lower levels (Orlanski and Chang 1993) and that is outside the region where wave activity is well defined (cf. section 2b).

The fraction of the linear eddy energy flux that is accounted for by the ageostrophic geopotential flux and the fraction of wave activity flux that is accounted for by its stationary component $\mathbf{W}_s$ can be compared directly in Fig. 9i. While eddy energy dispersion varies from about 5%–25%, the dispersive component of wave activity remains between 25% and 35%. In this case, the linear wave activity flux partitioning seems quite consistent with that of the idealized baroclinic flows examined by Chang and Orlanski (1994). Moreover, this partitioning appears to be relatively uniform throughout the length of the wave packet (Fig. 9h). The flux partitioning based on eddy energy also appears consistent with the importance of a dispersive energy flux, both at the leading edge and in the center of the wave packet (Fig. 9g), but owing to strong phase variations, the overall contribution is moderate. We may speculate, based on Fig. 9i, that the slow movement of this wave packet is related to the weak dispersion of eddy energy.

4. Discussion of nonlinearities

It is appropriate to emphasize that although we apply small-amplitude diagnostics to the evolution of 8–13 March, this event is perhaps better characterized as a large-amplitude event that involves nonlinearity and wave breaking. One indication of this is revealed by eddy energy dispersing meridionally (Figs. 4f–j) and by subtle phase dependence in the meridional component of wave activity flux (Fig. 6). At 0000 UTC 10 March (Fig. 6c), wave activity fluxes are directed slightly equatorward at the leading and trailing edges of the wave packet and poleward in the middle. Magnusdottir and Haynes (1996) note that when small-amplitude, Eliassen–Palm diagnostics (e.g., Edmon et al. 1980) are applied to large-amplitude perturbations, it is possible to misdiagnose the meridional *advection* of wave activity as wave propagation. This interpretation presumably applies here as well.

Localization of the spatial extent of a wave packet seems particularly relevant to our linear diagnosis of the preceding section. However, a localization of the North Pacific wave packet becomes somewhat complicated as it nears a slowly moving trough and growing wave activity center near the west coast of North America (recall the discussion of Fig. 3). It is possible that this downstream feature evolves from a subtropical wave breaking event during 8–10 March, followed by either reflection (Brunet and Haynes 1996) or advection (Enomoto and Matsuda 1999) of wave activity back toward the midlatitudes. In other words, the continental wave activity center appears to form independently of the North Pacific wave packet, although the distinction between these features becomes ambiguous after 0000 UTC 11 March, when they start to merge (Fig. 6).

Although the wave activity centers over the North Pacific and North America appear distinct, it is possible that their initial dynamical connection is not well resolved by our linear diagnoses. A nonlinear wave activity diagnosis is beyond our scope, but Orlanski and Chang (1993) indicate that for nonlinear evolutions, $\mathbf{C}_{ge}$ provides an underestimate of the advection of eddy energy. They consider the full flow advection of eddy energy, instead of that defined by the mean flow (Pedlosky 1987, section 6). If this nonlinear group velocity is applied here, the zonal group velocity increases by about 5 m s^{-1}. The difference between linear and nonlinear energy fluxes (Fig. 9c) also appears smaller before 11 March than afterward. This is consistent with previous indications of the role of nonlinearity (e.g., Fig. 3). On the other hand, the nonlinear group velocity exceeds all linear estimates (Fig. 9b), including the observed movement of the wave packet (Fig. 8). This is suggestive of a dynamical connection to the North American wave activity center that may not be well resolved.

While it may be relevant, in general, to distinguish nearby wave packets with separate identities, it is not clear whether this is feasible using conventional methods. Figure 10 compares the wave packets of the preceding section with those based on a complex demodulation of the eddy meridional wind (Bloomfield 1976) and a Hilbert transform of the meridional wind (Zimin et al. 2003). These fields are averaged between 600 and 100 hPa to be consistent with the vertical average of wave activity. We subjectively choose the 30 m s^{-1} contour to represent the complex demodulated wave packet (Fig. 10b) and for the slightly weaker Hilbert transform, a contour of 25 m s^{-1} is employed (Fig. 10d). Of these two methods, the Hilbert transform is more successful in resolving the temporal continuity of the wave packet (not shown).

Both the complex demodulation and Hilbert transform techniques include the eastern Pacific ridge axis at 0000 UTC 10 March. They also begin to include part of the trough that, according to a linear wave activity diagnosis, represents a dynamically independent feature over the west coast of North America. It is notable that wave breaking is not very pronounced at this time, which indicates that the two wave activity centers may indeed have separate identities to begin with. On the other hand, there is the suggestion of an eddy energy center across the ridge axis that is growing by energy propagation. These results highlight that further comparison of techniques to isolate a wave packet (including those based on the presence of wavy flows) are of interest. A closer examination of nonlinearity in the generation of wave activity over western North America may also be instructive in this case (cf. Magnusdottir and Haynes 1996).

5. Conclusions

Reexamination of a good example of downstream baroclinic development reveals the wave activity of TN01 to be a powerful complement to an eddy energy diagnosis. It provides a convenient means of identifying downstream development and its relevance to the growth of an eastern North Pacific cyclone. With respect to idealized wave trains of potential vorticity

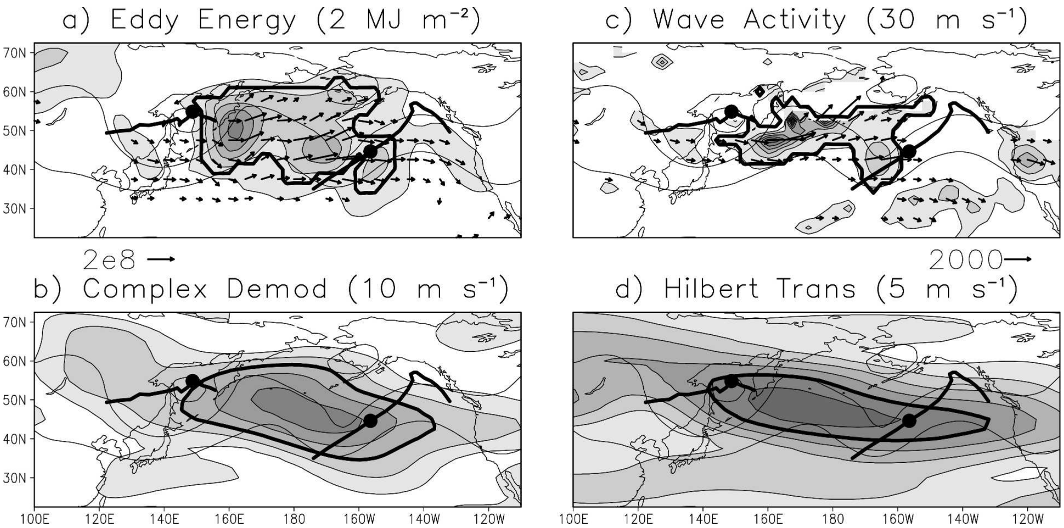

FIG. 10. Comparison of wave packets at 0000 UTC 10 Mar 1977 identified using (a) eddy energy, (b) complex demodulation of the eddy meridional wind, (c) wave activity, and (d) Hilbert transform of the full meridional wind. Eddy energy and wave activity are shown as in Fig. 8. Complex demodulated and Hilbert transformed wind fields are averaged between 600 and 100 hPa and contoured at 10 and 5 m s^{-1} intervals, respectively.

anomalies, the fundamental difference between eddy energy and wave activity is that the former captures only one phase of the entire wave packet, whereas TN01 emphasize that phase independence requires eddy potential enstrophy and its flux be considered as well. Although the physical interpretation of the ageostrophic geopotential flux and its divergence is well constrained (Chang and Orlanski 1994), this is generally not the case for the other eddy energy budget terms (Plumb 1983). Fortunately, such ambiguities do not necessarily complicate a diagnosis based on wave activity.

The evolution of interest is characterized by two troughs, associated with a western and an eastern North Pacific cyclone, that undergo wave breaking as eddy energy shifts downstream between adjacent eddy energy centers. The role of energy propagation to the sequential growth and decay of these energy centers is determined relative to the other energy budget terms. We find most terms to be smaller than positive contributions by the ageostrophic geopotential flux divergence term.

Using the wave activity of TN01, agreement is found with the direction that eddy energy disperses and the component of wave activity flux relative to the time-mean propagation of the eddies. Baroclinic conversion and the vertical flux divergence of wave activity are consistent insofar as these are relatively strong near the western cyclone. A contiguous wave packet should be collocated with both western and eastern cyclones if downstream development is relevant, and such a criterion is met here. The surface cyclones thus appear to represent two local sources of wave activity in the western and central North Pacific that feed a lengthening wave packet dominated by horizontal wave activity fluxes.

A direct comparison between eddy energy and wave activity group velocities reveal minor differences prior to wave breaking at upper levels. Comparisons with other events may help to clarify this result. Initially, good agreement is obtained by the two linear measures of local group velocity, when averaged over the wave packet of interest. Because the wave activity of Takaya and Nakamura (2001) is phase-independent, we also tracked the approximate center of the wave packet, which moves at about 22 m s^{-1} downstream. Our estimate of group velocity using eddy energy is the same as this, while wave activity indicates a slightly slower propagation.

The fraction of zonal eddy energy and wave activity propagation accounted for by the dispersive component has also been examined. Perhaps surprisingly, the wave activity flux partitioning of Chang and Orlanski (1994) seems consistent with that of idealized baroclinic flows, though not just at the leading edge of the wave packet but throughout its extent. Finally, we compared techniques for distinguishing between wave packets that appeared to have different origins. Both complex demodulation and the Hilbert transform seemed to resolve only approximately the main wave packet and another near the North American west coast. The results of this study help to clarify the role of downstream baroclinic development across the North Pacific Ocean. We cannot discount the possibility that basic-state conditions exist for which discrepancies between these two

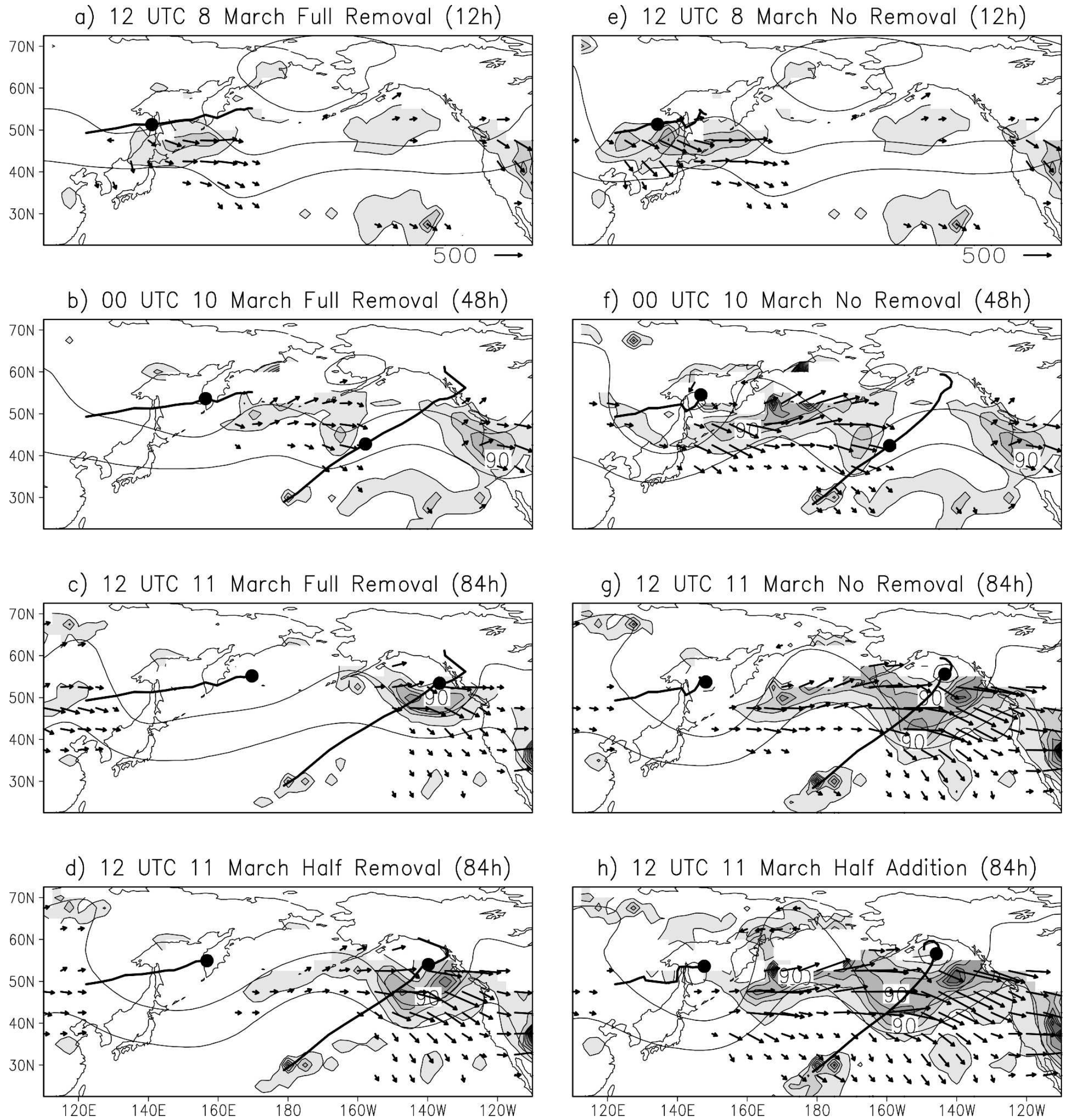

FIG. A1. Evolution of wave activity for the simulations described in Part I, including (top half) the full removal and no removal simulations and (bottom half) a comparison for all four simulations: vertical averages of wave activity and the stationary wave activity flux ($\mathbf{W}_s$) as in Fig. 6, but for the (a)–(c) full removal, (d) half removal, (e)–(g) no removal (control), and (h) half addition simulations. These are shown at (a), (e) 1200 UTC 8 Mar, (b), (f) 0000 UTC 10 Mar, and otherwise at 1200 UTC 11 Mar 1977.

diagnoses can be found, but certainly during the early evolution of the wave packet examined here, wave activity and eddy energy diagnoses appear to be in good agreement.

Acknowledgments. Comments on this study and on Part I by three anonymous reviewers helped to strengthen our presentation, and these are gratefully acknowledged. This research has been sponsored by the Natural Sciences and Engineering Research Council, Environment Canada, and the Canadian Foundation for Climate and Atmospheric Sciences. Gridded data were obtained through the Climate Diagnostics Center at Boulder, Colorado. Data visualization and feature tracking were facilitated by the GrADS software obtained from the Institute of Global Environment and Society at Calverton, Maryland.

APPENDIX

Dynamical Impact on the Evolution of Wave Activity

One benefit of viewing downstream baroclinic development in terms of the wave activity of TN01 is that interactions involving wave packet propagation are readily appreciated. In Part I, it was suggested that perturbations to an upstream ridge and trough couplet constitute an impact on the wave packet that defines both the western and eastern cyclones. It is instructive to complete a diagnosis of the North Pacific wave packet of 8–13 March 1977 by reexamining the four simulations of Part I in terms of wave activity. This can be compared with the eddy kinetic energy evolution in Fig. 7 of Part I.

The evolution of wave activity in the full removal simulation is shown in Figs. A1a–c. Removal of the Siberian ridge and trough couplet is by way of a direct modification of eddy enstrophy, which defines one phase of the TN01 wave activity (10). A comparison with the no removal simulation (Fig. A1e) reveals that it is primarily the enstrophy of the western trough that is modified. As a result, the full removal wave packet remains compact as it propagates eastward. This lack of a zonally extensive wave packet is another indication that it is partly fed by upward wave activity fluxes of the western cyclone (cf. section 3b). Both wave activity and its fluxes are considerably reduced as the eastern cyclone reaches maximum intensity.

The control simulation (Figs. A1e–g) is associated with robust wave activity fluxes that extend the wave packet downstream. In this case, upward wave activity fluxes near the eastern cyclone are also an important source (not shown). The half removal and half addition simulations at 1200 UTC 11 March are given in Fig. A1. As expected from the evolution of eddy energy, there is good correspondence between perturbations to the upstream ridge and trough couplet and the evolution of wave activity across the North Pacific Ocean. These results provide further support of an important dynamical connection between the eastern and western cyclones.

REFERENCES

Bloomfield, P., 1976: *Fourier Analysis of Time Series: An Introduction.* Wiley-Interscience, 258 pp.

Brunet, G., and P. H. Haynes, 1996: Low-latitude reflection of Rossby wave trains. *J. Atmos. Sci.,* **53,** 482–496.

Chang, E. K. M., 1993: Downstream development of baroclinic waves as inferred from regression analysis. *J. Atmos. Sci.,* **50,** 2038–2053.

——, 2000: Wave packets and life cycles of troughs in the upper troposphere: Examples from the Southern Hemisphere summer season of 1984/85. *Mon. Wea. Rev.,* **128,** 25–50.

——, 2001: The structure of baroclinic wave packets. *J. Atmos. Sci.,* **58,** 1694–1713.

——, and I. Orlanski, 1994: On energy flux and group velocity of waves in baroclinic flows. *J. Atmos. Sci.,* **51,** 3823–3828.

——, and D. B. Yu, 1999: Characteristics of wave packets in the upper troposphere. Part I: Northern Hemisphere winter. *J. Atmos. Sci.,* **56,** 1708–1728.

Danielson, R. E., J. R. Gyakum, and D. Straub, 2004: Examples of downstream baroclinic development among 41 cold-season eastern North Pacific cyclones. *Atmos.–Ocean,* **42,** 235–250.

——, ——, and ——, 2006: A case study of downstream baroclinic development over the North Pacific Ocean. Part I: Dynamical impacts. *Mon. Wea. Rev.,* **134,** 1534–1548.

Edmon, H. J., B. J. Hoskins, and M. E. McIntyre, 1980: Eliassen–Palm cross sections for the troposphere. *J. Atmos. Sci.,* **37,** 2600–2616.

Enomoto, T., and Y. Matsuda, 1999: Rossby wavepacket propagation in a zonally-varying basic flow. *Tellus,* **51A,** 588–602.

Hakim, G. J., 2000: Climatology of coherent structures on the extratropical tropopause. *Mon. Wea. Rev.,* **128,** 385–406.

——, 2003: Developing wave packets in the North Pacific storm track. *Mon. Wea. Rev.,* **131,** 2824–2837.

Hoskins, B. J., 1990: Theory of extratropical cyclones. *Extratropical Cyclones: The Erik Palmén Memorial Volume,* C. W. Newton, and E. O. Holopainen, Eds., Amer. Meteor. Soc., 63–80.

Joung, C. H., and M. H. Hitchman, 1982: On the role of successive downstream development in East Asian polar air outbreaks. *Mon. Wea. Rev.,* **110,** 1224–1237.

Kalnay, E., and Coauthors, 1996: The NCEP/NCAR 40-Year Reanalysis Project. *Bull. Amer. Meteor. Soc.,* **77,** 437–471.

Lackmann, G. M., D. Keyser, and L. F. Bosart, 1999: Energetics of an intensifying jet streak during the Experiment on Rapidly Intensifying Cyclones over the Atlantic (ERICA). *Mon. Wea. Rev.,* **127,** 2777–2795.

Lee, S., and I. M. Held, 1993: Baroclinic wave packets in models and observations. *J. Atmos. Sci.,* **50,** 1413–1428.

Longuet-Higgins, M. S., 1964: On group velocity and energy flux in planetary wave motions. *Deep-Sea Res.,* **11,** 35–42.

Magnusdottir, G., and P. H. Haynes, 1996: Wave activity diagnostics applied to baroclinic wave life cycles. *J. Atmos. Sci.,* **53,** 2317–2353.

Orlanski, I., 1994: Energy dispersion vs baroclinic conversion in the life cycle of atmospheric eddies. *Proc. Int. Symp. on Life Cycles of Extratropical Cyclones,* Vol. II, Bergen, Norway, Aase Grafiske A/S, 313–317.

——, and J. Katzfey, 1991: The life cycle of a cyclone wave in the Southern Hemisphere. Part I: Eddy energy budget. *J. Atmos. Sci.,* **48,** 1972–1998.

——, and E. K. M. Chang, 1993: Ageostrophic geopotential fluxes in downstream and upstream development of baroclinic waves. *J. Atmos. Sci.,* **50,** 212–225.

——, and J. P. Sheldon, 1993: A case of downstream baroclinic development over western North America. *Mon. Wea. Rev.,* **121,** 2929–2950.

——, and ——, 1995: Stages in the energetics of baroclinic systems. *Tellus,* **47A,** 605–628.

Pedlosky, J., 1987: *Geophysical Fluid Dynamics.* 2d ed. Springer–Verlag, 710 pp.

Plumb, R. A., 1983: A new look at the energy cycle. *J. Atmos. Sci.,* **40,** 1669–1688.

——, 1986: Three-dimensional propagation of transient quasi-geostrophic eddies and its relationship with the eddy forcing of the time-mean flow. *J. Atmos. Sci.,* **43,** 1657–1678.

Takaya, K., and H. Nakamura, 1997: A formulation of a wave-activity flux for stationary Rossby waves on a zonally varying basic flow. *Geophys. Res. Lett.,* **24,** 2985–2988.

——, and ——, 2001: A formulation of a phase-independent wave-activity flux for stationary and migratory quasigeostrophic eddies on a zonally varying basic flow. *J. Atmos. Sci.,* **58,** 608–627.

Thorncroft, C. D., B. J. Hoskins, and M. E. McIntyre, 1993: Two paradigms of baroclinic-wave life-cycle behaviour. *Quart. J. Roy. Meteor. Soc.,* **119,** 17–55.

Vanneste, J., and T. G. Shepherd, 1998: On the group-velocity property for wave-activity conservation laws. *J. Atmos. Sci.,* **55,** 1063–1068.

Zimin, A. V., I. Szunyogh, D. J. Patil, B. R. Hunt, and E. Ott, 2003: Extracting envelopes of Rossby wave packets. *Mon. Wea. Rev.,* **131,** 1011–1017.